Electrochemistry of the Nickel(II) Tris(2-diphenylphosphinoethyl)phosphine Halide Cations and an X-ray Crystallographic Structure of $[Ni(\eta^4\text{-}P_3P')Br][PF_6]\cdot{}^1/_2MeCN\cdot H_2O$

Tania Whyte,[†] Allan T. Casey,[†] and Geoffrey A. Williams*[,‡]

The School of Chemistry, University of Melbourne, Parkville, VIC 3052, Australia, and Australian Radiation Laboratory, Lower Plenty Road, Yallambie, VIC 3085, Australia

Received June 14, 1994[⊗]

The electrochemistry of the nickel(II) tris(2-diphenylphosphinoethyl)phosphine (P_3P') halide cations $[Ni(\eta^4\text{-}P_3P')X]^+$ (X = Cl, Br, I) has been studied in acetonitrile and dichloromethane. The cations undergo reduction to the nickel(0) $[Ni(\eta^4\text{-}P_3P')X]^-$ species. For the bromo and iodo complexes, reduction is followed by loss of halide and the formation of a P_3P'-bridged nickel(0) dimer. In acetonitrile $[Ni(\eta^4\text{-}P_3P')I]^+$ also loses iodide via a solvent exchange equilibrium. All the complexes are reversibly oxidized to the analogous nickel(III) species, and irreversibly oxidized to the corresponding nickel(IV) species. The structure of $[Ni(\eta^4\text{-}P_3P')Br][PF_6]\cdot{}^1/_2(MeCN)(H_2O)$ was determined by single-crystal X-ray crystallography. The complex crystallizes as dark purple plates in space group $P\bar{1}$, with two molecules in the unit cell, with $a = 10.171(7)$ Å, $b = 10.672(4)$ Å, $c = 21.040(8)$ Å, $\alpha = 87.27(3)°$, $\beta = 85.11(4)°$, $\gamma = 76.69(4)°$, and $R = 0.058$. X-ray photography indicates that although crystals are disordered, $[Ni(\eta^4\text{-}P_3P')I][PF_6]$ is isostructural with the bromo complex.

Introduction

The tetratertiary phosphine tris(2-(diphenylphosphino)ethyl)-phosphine (P_3P') coordinates to nickel(II) in a tetradentate fashion to give trigonal bipyramidal[1-4] species of the type $[Ni(\eta^4\text{-}P_3P')X]^{n+}$ where X = MeCN,[3] Cl,[1,2] Br, I,[2] or $P(OMe)_3$.[2] $[Ni(\eta^4\text{-}P_3P')(P(OMe)_3)]^{2+}$ has trigonal bipyramidal geometry[2] with the central P′ phosphorus of P_3P' and the $P(OMe)_3$ ligand in the axial positions and the three P phosphorus atoms of P_3P' in the equatorial positions. The three equatorial nickel–phosphorus distances are not equal and the nickel lies 0.12 Å below the equatorial plane, causing slight distortion from true trigonal bipyramidal C_{3v} symmetry.[5]

DuBois and Miedaner[3] have studied the reductive electrochemistry of $[Ni(\eta^4\text{-}P_3P')(MeCN)][BF_4]_2$ in acetonitrile solutions. They observed a pseudoreversible diffusion controlled one-electron reduction at −1.08 V vs $Fc^{+/0}$ and an irreversible reduction at −1.28 V vs $Fc^{+/0}$. They reported that at high concentrations this irreversible reduction was associated with electrode passivation and an oxidative spike on the reverse scan. DuBois and Miedaner also performed a bulk electrolysis at a mercury pool at −1.4 V vs $Fc^{+/0}$, which involved passage of 2.2 electrons per nickel atom and yielded a yellow precipitate. This was characterized by its phosphorus-31 NMR spectrum as a P_3P'-bridged nickel(0) dimer $[Ni(P_3P')]_2$.[3] A schematic structure of $[Ni(P_3P')]_2$ is shown below.

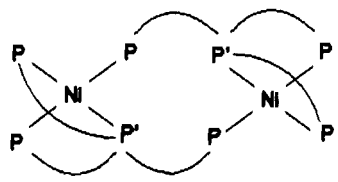

In this paper we report the electrochemistry and an X-ray crystallographic structure determination of the related nickel(II) P_3P' halide cations.

Results and Discussion

Electrochemistry. $[Ni(\eta^4\text{-}P_3P')Br][PF_6]$. Figure 1a shows a reductive cyclic voltammogram of a 1 mM solution of $[Ni(\eta^4\text{-}P_3P')Br][PF_6]$ in 1 mM Fc/0.1 M NBu_4PF_6/MeCN using a 0.86 mm platinum disk electrode at a scan rate of 0.25 V/s. In the reductive portion of the scan, there are two reductions, the first of which is labeled I′ and occurs as a shoulder at −1.09 V vs $Fc^{+/0}$ on the peak of the second, labeled II′, at −1.27 V vs $Fc^{+/0}$. Reduction II′ is partially reversible with the oxidation response II at −1.17 V vs $Fc^{+/0}$ on the reverse scan and a peak separation of 100 mV. Also on the reverse scan is a symmetrical absorption/desorption response at −1.02 V vs $Fc^{+/0}$ which makes it difficult to tell whether reduction I′ is reversible or not. In the oxidative portion of the voltammogram there are two irreversible oxidation processes, one at 0.38 V vs $Fc^{+/0}$ (VI) and one at 1.04 V vs $Fc^{+/0}$ (IV). There is also a couple at 0.60/0.53 V vs $Fc^{+/0}$ (III/III′) with a peak separation of 70 mV. The upper solvent limit is also present. Voltammograms where the potential is switched between processes III and IV show that couple III/III′ is reversible and a plot of peak current versus the square root of scan rate is linear, indicating that the process is diffusion controlled.

If the potential is switched after reduction I′ but before reduction II′ neither the absorption/desorption process at −1.02 V vs $Fc^{+/0}$ nor the oxidation process VI is observed. Thus each of these processes is due to species which are produced as a result of reduction II′. It is also clear from this experiment that reduction I′ is in fact irreversible under conventional conditions. Oxidative cyclic voltammograms of a solution identical to that in Figure 1a do not show process VI because reduction II′ has not been scanned first, but do show a new reduction process at −0.54 V vs $Fc^{+/0}$ (V′). If the potential is switched between oxidations III and IV, reduction V′ is absent so it arises from a species which is generated as a result of oxidation IV. Even at slow scan rates reductions I′ and II′ are poorly resolved from

* Author to whom correspondance should be addressed.
[†] University of Melbourne.
[‡] Australian Radiation Laboratory.
[⊗] Abstract published in *Advance ACS Abstracts,* March 15, 1995.

(1) King, R. B.; Kapoor, P. N.; Kapoor, R. N.; Saran, M. S. *Inorg. Chem.* **1971**, *10*, 1851.
(2) Hohman, W. H.; Kountz, D. J.; Meek, D. W. *Inorg. Chem.* **1986**, *25*, 616.
(3) DuBois, D. L.; Miedaner, A. *Inorg. Chem.* **1986**, *25*, 4642.
(4) King, R. B.; Cloyd, J. C. *Inorg. Chem.* **1975**, *14*, 1550.
(5) Gilheany, D. G. In *The Chemistry Of Organophosphorus Compounds*; Hartley, F. R., Ed.; Wiley & Sons: New York, **1990**, *1*, 9.

0020-1669/95/1334-2781$09.00/0

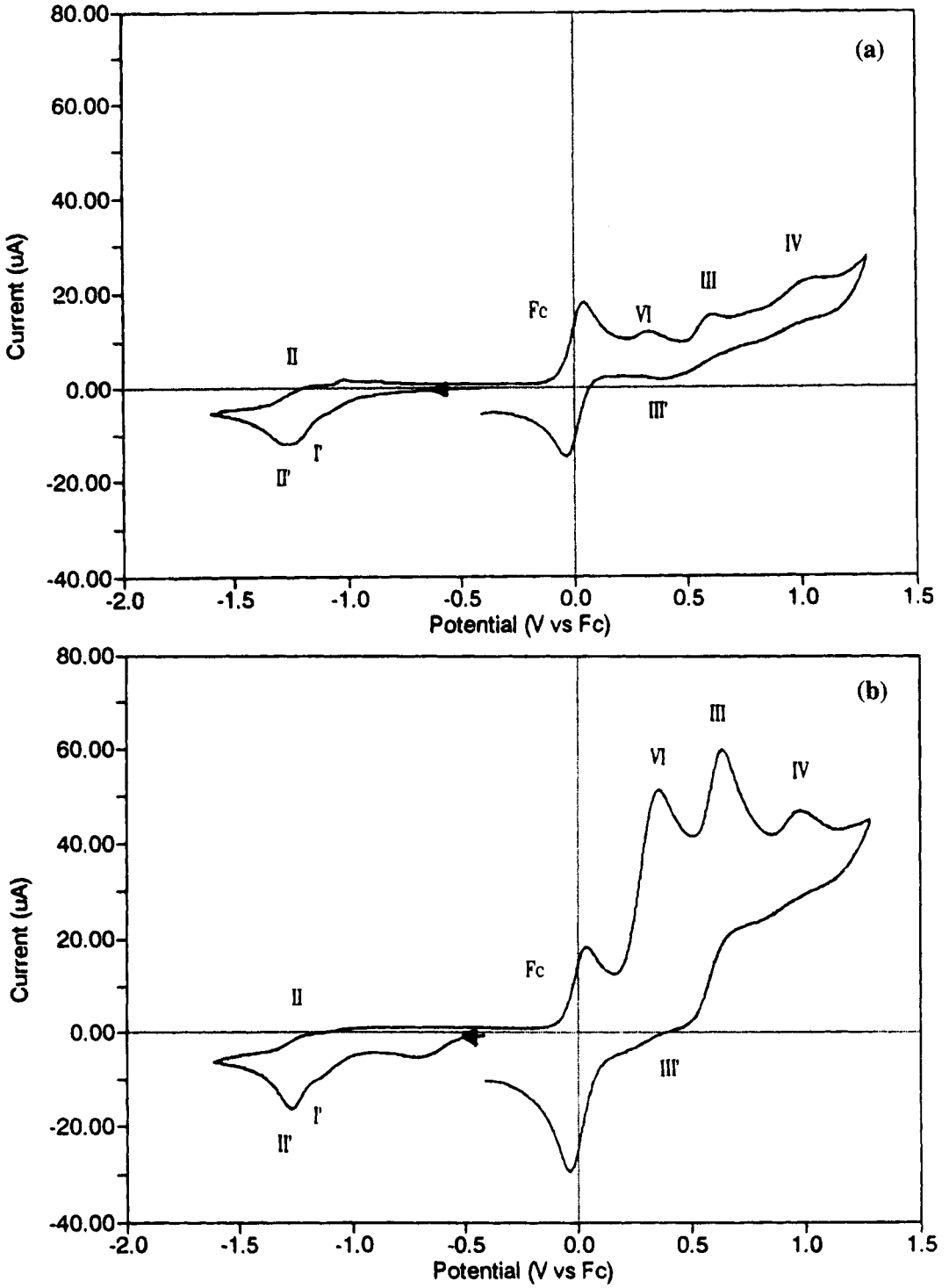

Figure 1. Reductive cyclic voltammograms of (a) [Ni(η^4-P_3P')Br][PF_6]: 1 mM in 1 mM Fc/0.1 M NBu_4PF_6/MeCN and (b) the same solution after addition of ca. 1 mM NBu_4Br, using a 0.86 mm radius platinum disk electrode at 0.25 V/s.

each other and at scan rates of 0.5 V/s or greater they are indistinguishable and appear as a composite process. As the scan rate is increased, the composite process gradually becomes more reversible until it appears as a single fully reversible couple at 130 V/s.

Controlled potential electrolysis of the deep purple [Ni(η^4-P_3P')Br][PF_6] at -1.4 V vs $Fc^{+/0}$ at a platinum gauze electrode in 0.1 M NBu_4PF_6/MeCN yielded a yellow precipitate at the working electrode and a yellow solution, with passage of 2.0 electrons per nickel atom. Processes I′ and II′ are therefore one-electron reductions and are assigned to the nickel(II)/nickel(I) and nickel(I)/nickel(0) reductions respectively. At scan rates less than 0.5 V/s, process I′ is irreversible while process II′ is partially reversible. At faster scan rates, reduction proceeds via a single two-electron process, which is fully chemically reversible only at the very fast scan rate of 130 V/s. The yellow precipitate is assumed to be responsible for the absorption/desorption response associated with process II′.

Oxidation VI is dependent on the nickel(I)/nickel(0) reduction II′. In the analogous [Ni(η^4-P_3P')(MeCN)]$^{2+}$ complex, the nickel(I)/nickel(0) reduction is followed by loss of acetonitrile and dimerisation.[3] If the bromo complex is to behave in the same way, loss of bromide would follow the nickel(I)/nickel(0) reduction. To test whether oxidation VI is due to the oxidation of free bromide, bromide addition experiments were performed. Cyclic voltammograms of NBu_4Br in 0.1 M NBu_4PF_6/MeCN show oxidative responses at 0.33 V vs $Fc^{+/0}$ and 0.63 V vs $Fc^{+/0}$ and reductive responses at 0.46 V vs $Fc^{+/0}$ and

Table 1. Electrochemical Data for the Nickel/P_3P' Complexes (ν = 0.25 V/s)

	peak potentials, E_p (V vs $Fc^{+/0}$)							
	Ni(0)/Ni(I)		Ni(I)/Ni(II)		Ni(II)/Ni(III)		Ni(III)/Ni(IV)	
acetonitrile solns	oxidn	redn	oxidn	redn	oxidn	redn	oxidn	redn
[Ni(η^4-P_3P')MeCN]$^{2+}$		−1.37		−1.01	0.58	0.48	0.90	0.73
[Ni(η^4-P_3P')Cl]$^+$	−1.24	−1.30	−1.03	−1.17	0.59	0.50	1.32	
[Ni(η^4-P_3P')Br]$^+$	−1.17	−1.27		−1.09	0.60	0.53	1.04	
[Ni(η^4-P_3P')I]$^+$	−1.07	−1.14		−0.95	0.65	0.58	1.33	

	Ni(0)/Ni(II)		Ni(II)/Ni(III)		Ni(III)/Ni(IV)	
dichloromethane solns	oxidn	redn	oxidn	redn	oxidn	redn
[Ni(η^4-P_3P')Cl]$^+$		−1.40	0.60	0.51	1.24	
[Ni(η^4-P_3P')Br]$^+$		−1.34	0.62	0.52	1.26	

	Ni(0)/Ni(I)		Ni(I)/Ni(II)		Ni(II)/Ni(III)		Ni(III)Ni/(IV)	
dichloromethane solns	oxidn	redn	oxidn	redn	oxidn	redn	oxidn	redn
[Ni(η^4-P_3P')I]$^+$	−1.22	−1.37		−1.09	0.65	0.54	1.25	

−0.15 V vs $Fc^{+/0}$. Figure 1b shows the reductive cyclic voltammogram of the solution from Figure 1a after addition of approximately 1 mM NBu_4Br. There is significant enhancement of the process VI and III peaks at 0.38 V vs $Fc^{+/0}$ and 0.61 V vs $Fc^{+/0}$ respectively. This indicates that process VI is due to the oxidation of free bromide in solution, while the peak labeled III is in fact due to oxidation of both [Ni(η^4-P_3P')Br]$^+$ and bromide, occurring at the same potential. Thus bromide is released into solution after [Ni(η^4-P_3P')Br]$^+$ undergoes the nickel(I)/(0) reduction process II′, in a reaction pattern similar to that of [Ni(η^4-P_3P')(MeCN)]$^{2+}$. It is therefore proposed that the yellow complex formed during the controlled potential electrolysis experiment is in fact the [Ni(P_3P')]$_2$ dimer reported by DuBois and Miedaner.[3] Attempts to collect the phosphorus-31 NMR spectrum of the extremely air-sensitive dimer were, however, unsuccessful.

The reductive reaction scheme for [Ni(η^4-P_3P')Br][PF_6] in acetonitrile solutions is thus as follows:

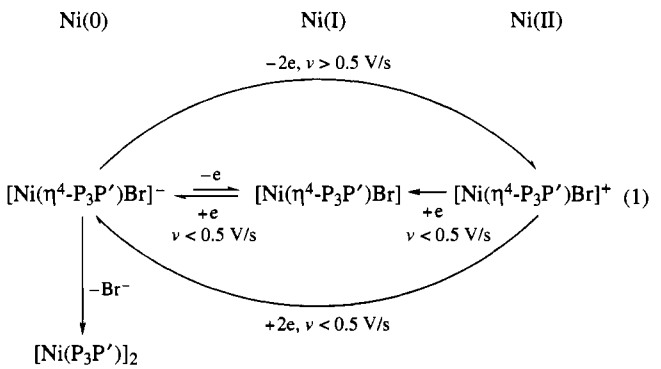

Couple III is assigned to the one-electron nickel(II)/(III) couple and the irreversible oxidation process IV is assigned to the one-electron nickel(III)/(IV) oxidation. The nickel(IV) species produced, [Ni(η^4-P_3P')Br]$^{3+}$ is not stable and one of its decomposition products undergoes reduction at −0.54 V vs $Fc^{+/0}$ to give process V′. Thus the oxidative electrochemical reaction scheme for [Ni(η^4-P_3P')Br][PF_6] in acetonitrile solutions is:

$$[Ni(\eta^4\text{-}P_3P')Br]^+ \underset{+e}{\overset{-e}{\rightleftharpoons}} [Ni(\eta^4\text{-}P_3P')Br]^{2+} \xrightarrow{-e} [Bi(\eta^4\text{-}P_3P')Br]^{3+} \quad (2)$$

Ni(II) Ni(III) Ni(IV)

A steady state voltammogram of the nickel(II)/nickel(III) oxidation of a 1 mM [Ni(η^4-P_3P')Br][PF_6] 0.1 M NBu_4PF_6/MeCN solution using a 0.57 μm radius platinum microelectrode has a limiting current of 0.088 nA. From this, the diffusion coefficient for the nickel(II) cation [Ni(η^4-P_3P')Br]$^+$ in 0.1 M NBu_4PF_6/MeCN was calculated[6] to be 4.0×10^{-10} m^2/s.

An oxidative cyclic voltammogram of a 1.29 mM solution of [Ni(η^4-P_3P')Br][PF_6] in 0.15 mM Fc/0.1 M NBu_4PF_6/CH_2Cl_2 using a 0.86 mm radius platinum electrode at a scan rate of 0.25 V/s shows an irreversible reduction at −1.34 V vs $Fc^{+/0}$ (I′), a reversible couple at 0.62/0.52 V vs $Fc^{+/0}$ (III/III′), an irreversible oxidation at 1.26 V vs $Fc^{+/0}$ (IV), and a reduction at −0.34 V vs $Fc^{+/0}$ (V′). If the potential is switched before oxidation IV, reduction V′ is absent. A reductive cyclic voltammogram of the same solution shows an extra oxidation response is present at 0.32 V vs $Fc^{+/0}$ (VI).

The electrochemical behavior of [Ni(η^4-P_3P')Br][PF_6] in dichloromethane is obviously very similar to that in acetonitrile (Table 1). The only difference to the overall pattern is that the reduction at −1.34 V vs $Fc^{+/0}$ (I′) is not split into two waves at slow scan rates. By analogy with the behavior of [Ni(η^4-P_3P')Br]$^+$ in acetonitrile, process I′ is assigned to the two-electron reduction of [Ni(η^4-P_3P')Br]$^+$ to [Ni(η^4-P_3P')Br]$^-$ while all the other processes are assigned in the same way as in the acetonitrile case.

In an oxidative steady state voltammogram of a 1.03 mM solution of [Ni(η^4-P_3P')Br][PF_6] in 0.1 M NBu_4PF_6/CH_2Cl_2 using a 0.57 μm radius platinum microelectrode, the nickel(II)/(III) oxidation process III appears as a sigmoidal curve but the wave associated with the nickel(III)/(IV) oxidation process IV is peak shaped. This indicates that process IV is too fast to achieve steady state conditions under these experimental conditions. The limiting current for the nickel(II)/nickel(III) oxidation is 0.906 nA and the diffusion coefficient for the nickel(II) cation, [Ni(η^4-P_3P')Br]$^+$ in 0.1 M NBu_4PF_6/CH_2Cl_2 is calculated[6] to be 5.6×10^{-10} m^2/s.

[Ni(η^4-P_3P')Cl][PF_6]. In 1 mM Fc/0.1 M NBu_4PF_6/MeCN solution [Ni(η^4-P_3P')Cl]$^+$ undergoes a partially reversible reduction at −1.23 V vs $Fc^{+/0}$ (I′/I), a reversible oxidation at 0.59/0.51 V vs $Fc^{+/0}$ (III/III′), and an irreversible oxidation at 1.32 V vs $Fc^{+/0}$ (IV). There is also an absorption/desorption response at −1.0 V vs $Fc^{+/0}$ and a reduction at −0.35 V vs $Fc^{+/0}$ (V′) which is dependant on first scanning oxidation process IV. By analogy with [Ni(η^4-P_3P')Br][PF_6], process I is assigned to the two-electron nickel(II)/nickel(0) reduction while processes III and IV are assigned to the one-electron nickel(II)/nickel(III) and nickel(III)/nickel(IV) oxidations. A steady state voltammogram

(6) Bond, A. M.;Oldham, K. B.; Zoski, C. G. *Anal. Chim. Acta* **1989**, *216*, 177.

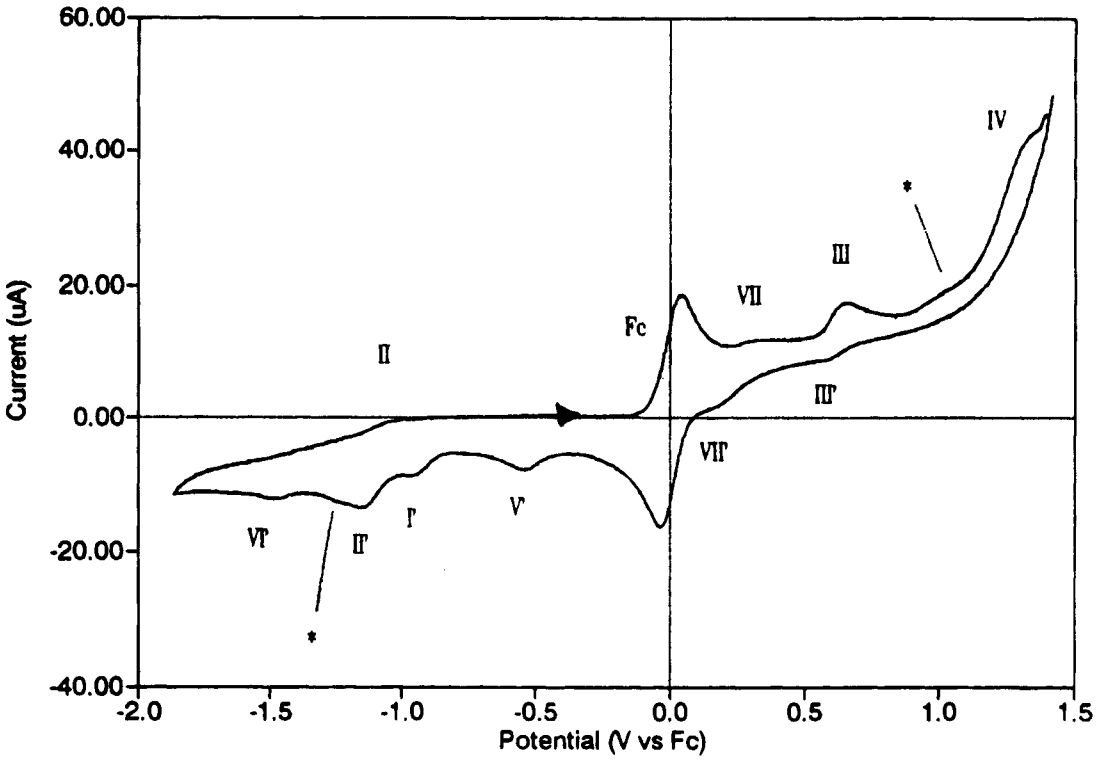

Figure 2. Oxidative cyclic voltammogram of $[Ni(\eta^4\text{-}P_3P')I][PF_6]$: 1 mM in 1 mM Fc/0.1 M NBu_4PF_6/MeCN using a 0.86 mm radius platinum disk electrode at 0.25 V/s.

of the nickel(II)/(III) oxidation yielded a limiting current of 0.716 nA at a 4.1 μm radius platinum microelectrode. From this the diffusion coefficient of $[Ni(\eta^4\text{-}P_3P')Cl]^+$ in 0.1 M NBu_4PF_6/MeCN was calculated[6] to be 4.6×10^{-10} m^2/s.

Cyclic voltammograms of NBu_4Cl in 0.1 M NBu_4PF_6/MeCN show oxidation waves at 0.37 V vs $Fc^{+/0}$ and 0.68 V vs $Fc^{+/0}$. There is no sign of an oxidation peak near 0.37 V vs $Fc^{+/0}$ in voltammograms of $[Ni(\eta^4\text{-}P_3P')Cl][PF_6]$, and addition of NBu_4Cl does not cause enhancement of any existing waves. Therefore there is no evidence to suggest that chloride is released into solution in a behavior analogous to that of $[Ni(\eta^4\text{-}P_3P')Br][PF_6]$.

The electrochemistry of $[Ni(\eta^4\text{-}P_3P')Cl][PF_6]$ in 0.1 M NBu_4PF_6/CH_2Cl_2 solutions differs only from that in acetonitrile in that the nickel(II)/nickel(0) reduction is irreversible in dichloromethane. Steady state voltammograms using the 4.1 μm radius platinum mircoelectrode yielded limiting currents of 1.468 nA for the nickel(II)/nickel(0) reduction and 0.741 nA for the nickel(II)/nickel(III) oxidation. These values give calculated[6] diffusion coefficients for $[Ni(\eta^4\text{-}P_3P')Cl][PF_6]$ in 0.1 M NBu_4PF_6/CH_2Cl_2 which differ by less than 1% and are 8.4×10^{-10} m^2/s and 8.5×10^{-10} m^2/s respectively.

$[Ni(\eta^4\text{-}P_3P')I][PF_6]$. Figure 2 shows an oxidative cyclic voltammogram of a 0.95 mM solution of $[Ni(\eta^4\text{-}P_3P')I][PF_6]$ in 0.1 M NBu_4PF_6/1 mM Fc/MeCN using a platinum electrode of radius 0.86 mm at a scan rate of 0.25 V/s. There are many peaks in the voltammogram but reduction processes I′ and II′ at −0.95 V vs $Fc^{+/0}$ and −1.14 V vs $Fc^{+/0}$, respectively, the reversible couple III/III′ at 0.65/0.58 V vs $Fc^{+/0}$, the irreversible oxidation IV at 1.33 V vs $Fc^{+/0}$, and the reduction V′ at −0.54 V vs $Fc^{+/0}$ are all familiar from the chloro and bromo systems. The processes which are unique to the iodo system are the reduction process VI′ at −1.47 V vs $Fc^{+/0}$ and the reversible couple VII/VII′ at 0.33/0.18 V vs $Fc^{+/0}$. There is also another oxidation process at 0.01 V vs $Fc^{+/0}$ which is masked in Figure 2 by the ferrocene oxidation peak. Addition of NBu_4I causes enhancement of these four peaks, indicating that they are due to the presence of iodide in solution. Controlled potential electrolysis of a of a 0.1 M NBu_4PF_6/MeCN solution of $[Ni(\eta^4\text{-}P_3P')I][PF_6]$ at −1.5 V vs $Fc^{+/0}$ yielded a yellow precipitate at the working electrode so it is proposed that $[Ni(\eta^4\text{-}P_3P')I]^+$ behaves in the same manner as $[Ni(\eta^4\text{-}P_3P')Br]^+$ in acetonitrile and loses iodide to form the yellow $[Ni(P_3P')]_2$ dimer following reduction to the nickel(0) species $[Ni(\eta^4\text{-}P_3P')I]^-$[1].

Unlike the bromo system, the iodide peaks are observed in oxidative voltammograms of fresh solutions where no reduction has taken place. This is probably due to a small amount of the iodo complex undergoing solvent exchange:

$$[Ni(\eta^4\text{-}P_3P')I]^+ + MeCN \rightleftharpoons [Ni(\eta^4\text{-}P_3P')(MeCN)]^{2+} + I^- \quad (3)$$

If this equilibrium is occurring, there should be peaks due to the oxidation and reduction of $[Ni(\eta^4\text{-}P_3P')(MeCN)]^{2+}$ in the voltammograms. Table 1 shows that while the nickel(II) oxidation and reduction potentials of $[Ni(\eta^4\text{-}P_3P')(MeCN)]^{2+}$ are close to those of $[Ni(\eta^4\text{-}P_3P')I]^+$ and would be masked by the iodo system peaks, the nickel(III)/(IV) oxidation and the nickel(I)/nickel(0) reduction occur at quite different potentials in the two systems. Careful examination of Figure 2 yields a small peak at ≈0.9 V vs $Fc^{+/0}$ labeled with an asterisk, which corresponds to the nickel(III)/nickel(IV) oxidation potential of the $[Ni(\eta^4\text{-}P_3P')(MeCN)]^{2+}$ system. There is also a hint of a shoulder on the process II′ peak at ≈−1.3 V vs $Fc^{+/0}$, also labeled with an asterisk, which corresponds well to the nickel(I)/nickel(0) reduction potential of the $[Ni(\eta^4\text{-}P_3P')(MeCN)]^{2+}$ system. The redox chemistry of $[Ni(\eta^4\text{-}P_3P')I][PF_6]$ in acetonitrile solutions therefore occurs in conjunction with the ligand exchange equilibrium in eq 3. However, the peaks due to the redox chemistry of $[Ni(\eta^4\text{-}P_3P')(MeCN)]^{2+}$ are small, so the equilibrium must lie to the left and $[Ni(\eta^4\text{-}P_3P')I]^+$ is the main nickel(II) species in solution.

The electrochemistry of $[Ni(\eta^4\text{-}P_3P')I][PF_6]$ in 0.1 M NBu_4PF_6/CH_2Cl_2 solutions differs from that in acetonitrile solutions only in that there is no iodide present in solution before reduction

Table 2. Crystallographic Details for [Ni(η^4-P_3P')Br][PF_6]·$^1/_2$(MeCN)(H_2O)

molecular formula	$C_{43}H_{45.5}BrF_6N_{0.5}NiOP_5$	F(000)	1014
M_r	992.79	μ (cm^{-1})	36.94
cryst descripn	dark purple plate	transmn factors min, max	0.659, 0.929
cryst syst	triclinic		
space Group	$P\bar{1}$	θ limits (deg)	1.5−65
a (Å)	10.171(7)	hkl range	h(0,11), k(±11), l(±23)
b (Å)	10.672(4)	no. of reflcns measd	6117
c (Å)	21.040(8)	no. of unique reflcns	3902
α (deg)	87.27(3)	structure solution	heavy atom method
β (deg)	85.11(4)	R_{merge}	0.032
γ (deg)	76.69(4)	no. of reflcns used	3149
unit cell vol (Å^3)	2213.4	no. of params	523
Z	2	refinement	blocked least squares (Fn minimized was $\sum w\Delta^2$)
D_o (g/cm^3)	1.45 (at 293.5 K)		
D_c (g/cm^3)	1.49 (at 295 K)	weighting scheme	$w = k/(\sigma_F^2 + g\lvert F_o\rvert^2)$
cryst dimens (distance in mm from centroid)	±(100) 0.186	final k	4.4773
	±(010) 0.058	final g	0.0003
	±(001) 0.010	final R (=$\sum\Delta/\sum\lvert F_o\rvert$)[a]	0.058
temp (K)	295−296	final R_w (=$[\sum w\Delta^2/\sum wF_o^2]^{1/2}$)	0.065
radiation/wavelength (Å)	Cu Kα 1.5418 (Ni filtered)	goodness of Fit	2.08
instrument	Siemens AED	max shift/esd	
scan type	θ: 2θ	nonsolvent	0.19
scan rate (deg/min)	2.5	solvent	0.66
θ scan width (deg)	[1.3 + 0.3 tan(θ)]	min. residual electron density, (e/Å^3)	−0.544
no. of intens controlled reflcns	3 every 50 (no significant variations)	max. residual electron density, (e/Å^3)	0.653

[a] $\Delta = \lvert\lvert F_o\rvert - \lvert F_c\rvert\rvert$.

to nickel(0) has occurred. The peak potentials for the various processes are listed in Table 1.

[Ni(η^4-P_3P')(MeCN)][BF_4]. The reductive electrochemistry of [Ni(η^4-P_3P')(MeCN)][BF_4] in acetonitrile was reported by DuBois and Miedaner[3] and is discussed in the Introduction to this paper. Oxidative cyclic voltammograms of 1 mM [Ni(η^4-P_3P')(MeCN)][BF_4] in 1 mM Fc/0.1 M NBu_4PF_6/MeCN show two pseudoreversible couples at 0.58/0.48 V vs $Fc^{+/0}$ (III/III') and 0.90/0.73 V vs $Fc^{+/0}$ (IV/IV'). There is also a small reductive wave at −0.51 V vs $Fc^{+/0}$ (V') which is dependant on first scanning couple IV. Couples III and IV are assigned to the one-electron nickel(II)/nickel(III) and nickel(III)/nickel(IV) couples, respectively.

Conclusion. The solvent plays a role in the loss of halide from the [Ni(η^4-P_3P')X]$^{n+}$ cations. In the [Ni(η^3-P_2P')Cl]$^+$ species the electrochemistry suggests that chloride is tightly bound and is not released into solution in either acetonitrile or dichloromethane, even after reduction to the nickel(0) species. In [Ni(η^4-P_3P')Br]$^+$, the bromide is stable in the nickel(II) species but is released following reduction to the nickel(0) species in both solvents. In [Ni(η^4-P_3P')I]$^+$, the iodide is less tightly bound again, and in acetonitrile a small amount is lost spontaneously via exchange with the solvent. The rest of the iodide is lost following reduction to the nickel(0) species. In dichloromethane, where solvent exchange is not possible, the iodide is not released into solution from the nickel(II) species, but is lost following reduction to the nickel(0) analog.

As may be seen in Table 1, the nickel(II)/nickel(I) and nickel(I)/nickel(0) reductions in acetonitrile become easier down the halogen group but the nickel(II)/nickel(III) couple remains the same within the limits of experimental error. The nickel(III)/nickel(IV) oxidation does not fit the overall pattern, in that the bromo compound is easier to oxidize than its chloro and iodo analogs. However, because these nickel(III)/nickel(IV) oxidation peaks occur as shoulders on the upper solvent limit, they are subject to larger experimental errors than the other peaks. In dichloromethane the iodo complex undergoes two one-electron reductions while the chloro and bromo complexes undergo a single two-electron reduction process. Again the oxidative behavior is virtually the same for all three halo compounds.

Crystallography. [Ni(η^4-P_3P')Br][PF_6]·$^1/_2$(MeCN)(H_2O) crystallised from acetonitrile as dark purple plates. Preliminary X-ray photography indicated that the crystal was triclinic. The structure was successfully solved in space group $P\bar{1}$ and refined to a final agreement index R = 0.058. The crystallographic data are listed in Table 2. The acetonitrile and water solvent molecules are disordered across the center of inversion and are not shown.

The cation in [Ni(η^4-P_3P')Br][PF_6]·$^1/_2$(MeCN)(H_2O) is singly charged so the gross crystal structure is different from that of [Ni(η^4-P_3P')($P(OMe)_3$)][AsF_6]$_2$·(MeOH)[2] which contains a dication and two [XF_6]$^-$ anions. However, the nickel cation structures of the two complexes display remarkably consistent geometries. Like the [Ni(η^4-P_3P')($P(OMe)_3$)]$^{2+}$ cation, the [Ni(η^4-P_3P')Br]$^+$ cation has distorted trigonal bipyramidal geometry with the P' phosphorus atom and the bromine atom in the axial positions. An Ortep[7] diagram of the [Ni(η^4-P_3P')Br]$^+$ cation is shown in Figure 3.

Table 3 lists the bond lengths and angles about the nickel center. The corresponding literature[2] values for [Ni(η^4-P_3P')($P(OMe)_3$)]$^{2+}$ are also listed for comparison. The three equatorial nickel−phosphorus bonds are of different lengths, Ni−P2 = 2.306(3) Å, Ni−P3 = 2.322(2) Å, and Ni−P4 = 2.251(3) Å, but they are all significantly longer than the axial Ni−P1 bond at 2.163(2) Å. The three P1−Ni−P_{eq} and the three P_{eq}−Ni−P_{eq} angles also vary and are consistent with those of [Ni(η^4-P_3P')($P(OMe)_3$)]$^{2+}$. As expected, the Ni−Br bond of 2.403(2) Å is significantly longer than the Ni−P* bond of 2.137(2) Å in [Ni(η^4-P_3P')($P(OMe)_3$)]$^{2+}$,[2] where P* is the phosphorus atom of the $P(OMe)_3$ ligand. A search of the Cambridge Structural Database[8] yielded eight structures containing five-coordinate nickel with phosphine or arsine ligands and a nickel−bromine bond. Several of these structures have trigonal bipyramidal geometry about the nickel center, but only two have bromine in an axial position. These are Ni($PP(Et)Ph_2)_3Br_2$ with Ni−Br_{ax} = 2.466(2) Å[9] and Ni[As(o-$C_6H_4AsPh_2)_2$(o-C_6H_4SMe)Br]$^+$ with Ni−Br = 2.341(2) Å.[10] The Ni−Br bond in [Ni(η^4-P_3P')Br]$^+$ falls between these two previous examples.

(7) Johnson, C. K. *Ortep II, A Fortran Thermal-ellipsoid Plot Program for Crystal Structure Illustrations;* Report ORNL-5138; Oak Ridge National Laboratory: Oak Ridge, TN, 1976.
(8) Allen, F. H.; Davies, J. E.; Galloy, J. J.; Johnson, O.; Kennard, O.; Macrae, C. F.; Mitchell, E. M.; Mitchell, G. F.; Smith, J. M.; Watson, D. G. *J. Chem. Inf. Comput. Sci.* **1991**, *31*, 187.
(9) Powell, H. M.; Watkin, D. J. *Acta Crystallogr.* **1977**, *B33*, 2294.

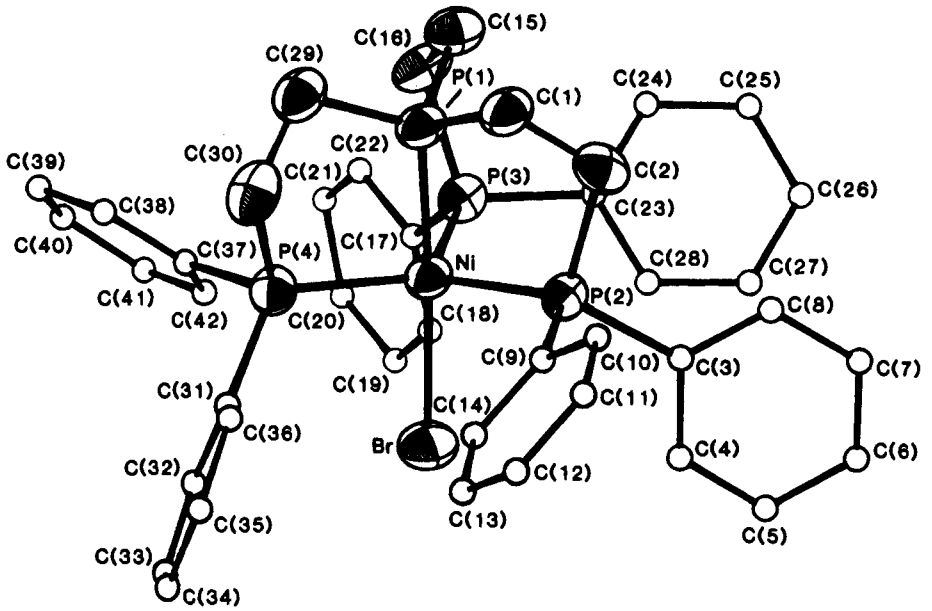

Figure 3. Ortep[7] diagram of the $[Ni(\eta^4\text{-}P_3P')Br]^+$ cation in $[Ni(\eta^4\text{-}P_3P')Br][PF_6]\cdot{}^1/_2(MeCN)(H_2O)$. Thermal ellipsoids, showing principal ellipses and axes, are drawn at the 50% probability level. The phenyl ring carbon atoms have been drawn with an arbitrary isotropic radius of 0.1 Å to allow a clear view of the trigonal bipyramidal coordination about the nickel center. The P′ phosphorus atom of P_3P' is numbered P1 while the three P phosphorus atoms are numbered P2, P3, and P4.

Table 3. Selected Bond Lengths (Å) and Angles (deg) for $[Ni(\eta^4\text{-}P_3P')Br][PF_6]\cdot{}^1/_2(MeCN)(H_2O)$ (See Figure 3 for Numbering of Atoms)

$[Ni(\eta^4\text{-}P_3P')Br]^+$				$[Ni(\eta^4\text{-}P_3P')(P(OMe)_3)]^{2+}$ data from ref 2	
Ni−Br	2.403(2)	P1−C1	1.817(10)	Ni−P* [a]	2.137(2)
Ni−P1 (P′)	2.163(2)	P1−C15	1.829(8)	Ni−P1 (P′)	2.181(2)
Ni−P2	2.306(3)	P1−C29	1.814(10)	Ni−P2	2.325(2)
Ni−P3	2.322(2)	P2−C2	1.839(8)	Ni−P3	2.275(2)
Ni−P4	2.251(3)	P3−C16	1.840(9)	Ni−P4	2.283(2)
P1−Ni−Br	176.6(1)	P4−C30	1.833(8)	P1−Ni−P*	175.8(1)
P2−Ni−Br	97.4(1)	C1−C2	1.528(11)		
P3−Ni−Br	95.6(1)	C15−C16	1.539(13)		
P4−Ni−Br	91.9(1)	C29−C30	1.535(14)		
P2−Ni−P1	84.9(1)	P2−C3	1.809(10)	P2−Ni−P1	86.3(1)
P3−Ni−P1	85.8(1)	P2−C9	1.838(8)	P3−Ni−P1	85.6(1)
P4−Ni−P1	84.7(1)	P3−C17	1.811(9)	P4−Ni−P1	84.2(1)
P2−Ni−P3	113.7(1)	P3−C23	1.824(10)	P2−Ni−P3	113.2(1)
P2−Ni−P4	120.4(1)	P4−C31	1.826(9)	P2−Ni−P4	121.9(1)
P3−Ni−P4	123.8(1)	P4−C37	1.825(10)	P3−Ni−P4	122.8(1)

[a] P* corresponds to P of $P(OMe)_3$.

Table 4. Atomic Positional Coordinates, with Esd Values, for Selected Atoms in $[Ni(P_3P')Br][PF_6]\cdot{}^1/_2(MeCN)(H_2O)$

atom	*X/a*	*Y/b*	*Z/c*
Ni	0.28946(13)	0.05190(12)	0.27723(6)
Br	0.17865(10)	0.16083(10)	0.37131(5)
P1	0.39867(23)	−0.04001(21)	0.19280(10)
P2	0.10343(22)	0.09005(21)	0.21770(10)
P3	0.33731(22)	−0.15212(21)	0.32540(10)
P4	0.43747(22)	0.18050(21)	0.26477(10)
C1	0.2885(9)	−0.0485(9)	0.1303(4)
C2	0.1711(9)	0.0704(9)	0.1340(4)
C15	0.4848(9)	−0.2060(8)	0.2118(4)
C16	0.3893(9)	−0.2638(8)	0.2591(4)
C29	0.5267(9)	0.0423(9)	0.1586(4)
C30	0.5835(9)	0.0971(9)	0.2138(4)

The nickel atom in $[Ni(\eta^4\text{-}P_3P')Br]^+$ lies 0.195(1) Å below the equatorial plane defined by P2, P3, and P4, where "below" indicates toward bromine. This displacement is greater than that observed in $[Ni(\eta^4\text{-}P_3P')(P(OMe)_3)]^{2+}$ where the nickel lies 0.12 Å below the equatorial plane.[2] In the aliphatic arms of the P_3P' ligand, the "upper" P1−carbon bonds, P1−C1, P1−C15, and P1−C29, are all slightly shorter than the "lower", P2−C2, P3−C16, and P4−C30, bonds. Planes drawn through P1, Ni, and each equatorial phosphorus in turn are named "P_{eq} slice" planes and the upper carbon atoms of the ligand arms are all displaced from their slice planes in an anticlockwise direction when viewed from above. The displacements are not the same but average 0.20 Å. The lower carbon atoms are displaced from the slice planes in a clockwise direction and have a much larger average displacement of 0.54 Å. Therefore, the P_3P' tripod ligand arms are buckled to accommodate the nickel center.

The bond lengths for the phenyl rings range between 1.35(2) and 1.42(1) Å and average 1.39(1) Å. The $[PF_6]^-$ anion has distorted octahedral geometry with P−F bonds averaging 1.53(1) Å and *cis*-F−P−F angles averaging 90.0°. The methyl carbon C43 of the disordered acetonitrile molecule lies at the crystallographic center of inversion. The C−C bond is 1.33(3) Å, and the C−N bond is 1.00(5) Å.

Several batches of $[Ni(\eta^4\text{-}P_3P')I][PF_6]$ crystals were grown from saturated acetonitrile environments and yielded intensely blue needles. Two crystals from different batches were photographed and while both gave acceptable oscillation photographs, the zero level Weissenberg photographs showed both crystals to be too disordered for worthwhile diffraction data collection. However, a limited amount of information was available from the photography. Assuming rotation about the *a* axis, $a = 10.16$ Å, $\alpha^* = 89°$, $b^* = 0.093$ Å^{-1}, and $c^* = 0.048$ Å^{-1}. These values are very similar to those for $[Ni(\eta^4\text{-}P_3P')Br][PF_6]\cdot{}^1/_2(MeCN)(H_2O)$: $a = 10.171$ Å, $\alpha^* = 91.66°$, $b^* = 0.096$ Å^{-1} and $c^* = 0.048$ Å^{-1}. Therefore, $[Ni(\eta^4\text{-}P_3P')I][PF_6]$ is clearly isostructural with the bromo complex.

Experimental Section

Chemicals. The polyphosphines were purchased from Strem and used as supplied. Other chemicals were purchased from normal suppliers.

Spectroscopy. Phosphorus-31 NMR studies were performed on a JEOL FX 100 spectrometer using an external lithium-7 lock and broadband proton decoupling. Electronic spectra were collected using a Hitachi 150−20 Spectrophotometer and Data Processor. Table 5 contains the spectroscopic data for the nickel complexes.

(10) Mathew, M.; Palenik, G. J.; Dyer, G.; Meek, D. W. *J. Chem. Soc., Chem. Commun.* **1972**, 379.

Table 5. Spectroscopic Data for the Nickel/P_3P' Complexes[a]

complex	δ(^{31}P) (ppm)			J (Hz)		λ_{max} (cm^{-1})	
	P′	P	P in PF_6	^3J(P′−P)	^1J(P−F)		
[Ni(η^4-P_3P')MeCN][BF_4]$_2$	142.0 q	33.4 d		29		18 200	35 500
[Ni(η^4-P_3P')Cl][PF_6]	140.4 q	32.3 d	−144.5 sp	29	708	18 100	34 200
[Ni(η^4-P_3P')Br][PF_6]	150.6 q	33.0 d	−144.6 sp	24	708	18 500	34 100
[Ni(η^4-P_3P')I][PF_6]	168.3 q	37.3 d	−144.5 sp	20	708	16 700	34 700

[a] Spectra were collected from dichloromethane solutions.

Crystallography. Crystals of [Ni(η^4-P_3P')Br][PF_6]·$^1/_2$(MeCN)(H_2O) were grown by slow evaporation of acetonitrile to yield purple needles. Deep blue needles of [Ni(η^4-P_3P')I][PF_6] were grown in the same manner but of two crystals photographed, both showed considerable disorder. Oscillation and Weissenberg photographs were taken using a Huber Weissenberg Goniometer, Model 102. Intensity data were collected on a Siemens AED 3-circle automated diffractometer using the parameters given in Table 2. Unit cell parameters, together with their esd's, were derived by a least-squares analysis[11] of the setting angles. These were determined on the diffractometer at 295 K with Cu Kα radiation (λ = 1.5418 Å) for 30 reflections with 2θ greater than 40°. The integrated intensities were corrected for Lorentz and polarisation effects, and for absorption.[12] The structure was solved by the heavy atom method using Shelx76[13] and Shelx400.[13] The refinement details are listed in Table 2. There was no evidence of secondary extinction effects. Neutral-atom scattering-factor curves for C, N, O, F, and P were taken from ref 14. Those for Br, H, and Ni were from refs 15−17 respectively. Real and imaginary anomalous dispersion corrections were applied to the non-hydrogen atoms.[12] Table 4 lists atomic coordinates for nickel and its coordination sphere in [Ni(η^4-P_3P')Br][PF_6]·$^1/_2$(MeCN)(H_2O).

Electrochemistry. AR grade dichloromethane was dried over alumina prior to use. HPLC grade acetonitrile was used as supplied. Tetrabutylammonium hexafluorophosphate, NBu_4PF_6, was used as a supporting electrolyte at concentrations between 0.1 and 0.5 M. Solutions were degassed with high purity nitrogen before all reductive experiments. All potentials are quoted relative to the half wave potential of the ferrocene/ferrocenium couple in volts versus ferrocene/ferrocenium, V vs $Fc^{+/0}$.[18] Where convenient, ferrocene was included in the test solutions as an internal reference.

A solution of ferrocene in 0.2 M lithium perchlorate/acetonitrile[19] was used to calibrate the nominal 0.9 mm and 5 μm radius platinum electrodes. The macroelectrode was calibrated by chronocoulometry (CC) and linear potential sweep voltammetry[18] and both techniques gave a radius of 0.86 mm. The microelectrode was calibrated by steady state voltammetry (SSV) and found to have a radius of 4.1 μm. These two electrodes were then used to measure the diffusion coefficient of ferrocene in 0.1 M NBu_4PF_6/MeCN, which was 2.3 × 10^{-9} m^2/s by both CC and SSV. The remaining microelectrodes were calibrated in 0.1 M NBu_4PF_6/MeCN by SSV.

Cyclic voltammetry and SSV were performed using a Cypress Electrochemical System Model CYSY1R with a three electrode configuration. The system includes a Cypress Picoamp Booster Model PTO11 which is used with microelectrodes to help collect small currents accurately. Controlled potential electrolysis experiments were carried out using a BAS 100 electrochemical analyzer. The working and auxiliary electrodes were platinum gauze and the auxiliary was separated from the test solution by a salt bridge. The reference electrode was silver/silver chloride which was also separated from the test solution by a salt bridge. The solution was maintained under an argon atmosphere and stirred throughout the electrolysis.

Preparations. NBu_4PF_6, tetrabutylammonium hexafluorophosphate was synthesized using a modified literature method.[20] Tetrabutylammonium iodide (50 g) and potassium hexafluorophosphate (26 g) were separately dissolved, with heating, in the minimum possible volumes of acetone. The two solutions were combined, and the resulting potassium iodide precipitate was filtered off. The solution was then treated with a large excess (ca. 2 L) of water to precipitate the crude product. This was collected, washed with water, and then dissolved in a solution of potassium hexafluorophosphate (10 g) in acetone (200 mL). The NBu_4PF_6 was reprecipitated with water, filtered off and washed with water, and allowed to dry at the pump for an hour. It was then recrystallized from hot ethanol/water and dried well before a second recrystallization from hot ethanol, followed by drying in vacuo at 70 °C for 2 h.

Spectroscopic data for the nickel complexes are listed in Table 5. [Ni(η^4-P_3P')MeCN][BF_4]$_2$ was synthesized by an electrolysis method.[21] A sacrificial nickel anode and a platinum cathode were immersed in a solution of P_3P' in NBu_4BF_4/MeCN under an argon atmosphere; the power source was a Bang & Olufson SN15 power supply. Current was passed until the initially clear solution had become dark purple, when it was filtered. The solvent was removed under vacuum, and the residue recrystallised from dichloromethane/hexane. This method has an advantage over the literature one[3] in that it does not require the preparation of [Ni(MeCN)$_6$](BF_4)$_2$·$^1/_2$MeCN as a precursor.[22]

[Ni(η^4-P_3P')X][PF_6] (X = Cl, Br). A solution of either $NiCl_2$·$6H_2O$ (0.1 g) or $NiBr_2$·$3H_2O$ (0.12 g) and P_3P' (0.3 g) in ethanol was refluxed for 1 h. NH_4PF_6 (excess) in water was added to the solution and the ethanol was removed under vacuum. The resulting precipitate was collected and washed with water before being redissolved in dichloromethane. The lower aqueous layer was discarded and hexane added to reprecipitate the product.

[Ni(η^4-P_3P')I][PF_6] was prepared by a slight adaptation of a literature method.[2] KI (0.17 g) and Ni(NO_3)$_2$·$6H_2O$ (0.29 g) were stirred in ethanol (25 mL) at room temperature overnight. The resulting KNO_3 was filtered off and discarded. To half of the pale green filtrate was added NH_4PF_6 (0.12 g), and P_3P' (0.34 g) in dichloromethane (5 mL), upon which the solution became dark blue. The solution was heated at 50 °C for an hour and then refluxed for 6 h. Half the solvent was allowed to evaporate, and the resulting [Ni(η^4-P_3P')I][PF_6] was filtered off.

Acknowledgment. T.W. thanks the Australian government for an APRA award and Dr. R. Gable and Ms. M. Hardie for their help in using the Ortep program.

Supplementary Material Available: Tables of atomic coordinates, anisotropic thermal parameters, additional bond distances and angles, and displacements from mean planes for the X-ray crystal structure of [Ni(η^4-P_3P')Br][PF_6]·$^1/_2$(MeCN)(H_2O) (7 pages). Ordering information is given on any current masthead page.

IC9406805

(11) Grant, D. F.; Gabe, E. J.; Le Page, Y. *Glsor Least Squares Orientation Matrix Program*; National Research Council of Canada: Ottawa, 1978.
(12) Cromer, D. T.; Liberman, D. *J. Chem. Phys.* **1970**, *53*, 1891.
(13) Sheldrick, G. M. *Program for Crystal Structure Determination*; University of Cambridge, Cambridge, England, 1976.
(14) Cromer, D. T.; Mann, J. B. *Acta Crystallogr.* **1968**, *A24*, 321.
(15) Doyle, P. A.; Turner, P. S. *Acta Crystallogr.* **1968**, *A24*, 390.
(16) Stewart, R. F.; Davidson, E. R.; Simpson, W. T. *J. Chem. Phys.* **1965**, *42*, 3175.
(17) Eds. Ibers, J. A.; Hamilton, W. C. *International Tables for X-ray Crystallography*; Kynoch Press: Birmingham, England, 1974; Vol. 4, 99−101.
(18) Rieger, P. H. *Electrochemistry*; Prentice-Hall: Princeton, New Jersey, 1987.
(19) Kuwana, T.; Bublitz, D. E.; Hoh, G. *J. Am. Chem. Soc.* **1960**, *82*, 5811.
(20) Eds. Kissinger, P. T.; Heineman, W. R. *Laboratory Techniques in Electroanalytical Chemistry*; Dekker: New York, 1984.
(21) Casey, A. T.; Vecchio, A. M. *Transition Met. Chem. (Weinheim, Ger.)* **1986**, *11*, 366.
(22) Hathaway, B. J.; Holah, D. G.; Underhill, A. E. *J. Chem. Soc.* **1962**, 2444.